Piriform cortex takes sides: temporally-segregated odor representations from ipsilateral and contralateral nostrils within a single sniff

Gulce Nazli Dikecligil[1]*, Andrew I Yang[2]*, Nisha Sanghani[1], Timothy Lucas[2], H. Isaac Chen[2], Kathryn A Davis[1], Jay A Gottfried[1, 3]

*Equal Contribution
[1]Department of Neurology, Perelman School of Medicine, University of Pennsylvania, Philadelphia, PA, 19104, USA
[2]Department of Neurosurgery, Perelman School of Medicine, University of Pennsylvania, Philadelphia, PA, 19104, USA
[3]Department of Psychology, School of Arts and Sciences, University of Pennsylvania, Philadelphia, PA, 19104, USA

Correspondence:
G. Nazli Dikecligil, PhD
Department of Neurology
Perelman School of Medicine
University of Pennsylvania
Philadelphia, PA 19104
Email: nazdikec@pennmedicine.upenn.edu

HIGHLIGHTS

- Ipsilateral odors are encoded faster than contralateral odors in piriform cortex
- Bi-nostril odors are encoded in two non-overlapping epochs within a single sniff
- Robustness of odor coding correlates with improved odor identification across subjects
- The timing of odor coding determines when piriform responses inform odor identification

SUMMARY

The human olfactory system has two discrete channels of sensory input, arising from olfactory epithelia housed in the left and right nostrils. Here, we asked whether primary olfactory cortex (piriform cortex, PC) encodes odor information arising from the two nostrils as unified or distinct stimuli. We recorded intracranial EEG signals directly from PC while human subjects participated in an odor identification task where odors were delivered to the left, right, or both nostrils. We analyzed the time-course of odor-identity coding using machine learning approaches, and found that odor inputs from the ipsilateral nostril are encoded ~480 ms faster than odor inputs from the contralateral nostril. This temporal staggering across the nostrils gave rise to two non-overlapping epochs of odor coding within a single sniff when odors were sampled through both nostrils. These findings reveal that PC maintains distinct representations from each nostril by temporally segregating odor information, highlighting an olfactory coding scheme at the cortical level that can parse odor information across nostrils within a single sniff.

INTRODUCTION

The human olfactory system has two discrete channels of sensory input within the nose. Olfactory epithelia in the left and right nostrils, isolated from one another by the nasal septum, each receive a snapshot of the sensory world upon inhalation. However, as odor stimuli in the natural environment can change rapidly over time and space[1–4], the olfactory composition of these two snapshots may vary considerably on any given sniff[5]. As such, while olfactory information arising from the two nostrils ultimately converges onto a unified odor percept, studies across animals and humans have shown that inter-nostril differences can also inform and shape behavior[6–9]. For instance, differences in odor concentration across the two nostrils help rodents localize an odor source[6] and can bias motion perception in humans towards the nostril with the higher concentration odorant[9]. Such findings strongly imply that the olfactory system is equipped both to integrate and segregate odor information arising from each side

of the nasal cavity. However, despite extensive work on odor responses in the olfactory system[10–15], relatively little is known about how information from the two nostrils is integrated and differentiated in the human olfactory system[16]. Specifically, if PC, a region critical for encoding odor identity information, favors integration or segregation of odor information across the two nostrils remains poorly understood.

The question of sensory integration across two discrete channels is particularly interesting in context of olfaction, as the ascending olfactory pathway from the periphery to PC is organized ipsilaterally: sensory neurons in each epithelium synapse onto glomeruli in the ipsilateral OB, which then project to ipsilateral PC[17]. Despite these prominent ipsilateral projections, interhemispheric communication at different stages of the olfactory pathway is thought to underlie sensory integration across nostrils[16,18–23]. Recent work outlining the interhemispheric connections in the rodent olfactory system indicates that odor information arising from the ipsilateral nostril reaches PC in just two synapses, whereas odor information arising from the contralateral nostril takes a more circuitous route[16], raising the intriguing possibility that odor information from the two nostrils may not reach PC simultaneously.

Single neuron recordings in rodents[21,22] and neuroimaging studies in humans[24,25] have shown that PC can respond to odors arising from either nostril, although the time course of these responses and its impact on sensory convergence across nostrils has not been investigated. Additionally, whether integration or segregation across nostrils underlies odor coding in the human PC is not known. Lastly, in contrast to rodents, relatively little is known about the neural circuitry of the human olfactory system and the pathways that support interhemispheric communication of olfactory information. One possibility is that odor information arising from each epithelium is integrated early in the processing stream, at the level of the OB, as proposed by recent work in rodents[20], such that odor information arriving at PC has already been unified across nostrils. Alternatively, inputs from each nostril might be represented as independent stimuli with distinct spatial and/or temporal response profiles, as a consequence of the putative differences between the ipsilateral and contralateral pathways[16].

In this study we set out to investigate if human PC maintains distinct and separable representations of odor information arising from each nostril. To this end, we recorded intracranial EEG (iEEG) signals in PC from patients undergoing epilepsy monitoring, enabling us to characterize odor responses with high spatial and temporal resolution. Subjects participated in an odor identification task where odors were delivered either to the left, right, or bilateral nostrils via a computer-controlled olfactometer. This approach allowed us to investigate the temporal evolution of odor coding in a nostril-dependent manner and to correlate odor responses with subjects' ability to identify odorants. We hypothesized that PC would temporally segregate odor information arising from the ipsilateral and contralateral nostrils and thus maintain distinct representations of odor identity for each nostril.

RESULTS

Experimental paradigm and behavioral performance

Ten subjects with intracranial depth electrodes participated in an odor identification task where odor stimuli were delivered either to the left, the right, or both nostrils (bi-nostril condition), via a computer-controlled olfactometer (Fig. 1A). Each trial began with a fixation cross, followed by a countdown and cue to sniff. Subjects received one of three unique odors or odorless air through one of the three nostril configurations (left, right, or bilateral), and were subsequently asked to identify the stimulus they received in a four-alternative forced-choice task (odor identity judgment). In a subset of trials, subjects were asked a follow-up question on whether they received the stimulus from left, right, or both nostrils (laterality judgment) (Fig. 1B). Local field potentials (LFPs) were recorded directly from the PC via intracranial depth electrodes throughout the duration of the task (Fig. 1C, D).

A summary of behavioral results for each nostril condition (e.g., left, right, and bilateral) is shown in Fig. 2. In addition, we report the averaged results from left and right nostril trials in the uni-nostril

condition to draw direct comparisons between the uni-nostril and bi-nostril conditions. Subjects correctly reported the presence of an odor in 84.9% ± 2.5%, 89.3% ± 4.2%, and 97.8% ± 1.0% of left, right, and bi-nostril trials, respectively (Fig. 2A, one-sample Wilcoxon signed rank test vs. 50% chance level, p = 0.002 for each nostril condition). Odor detection performance was higher for bi-nostril compared to uni-nostril trials, but there were no significant differences between the detection performance of left and right nostrils (two-sample Wilcoxon signed rank tests, p=0.002 and p>0.05, respectively).

For trials in which subjects correctly detected the presence of an odor, odor identification performance was 81.4% ± 4.7%, 81.7% ± 4.2%, and 87.4% ± 3.7% for left, right, and bi-nostril trials, respectively (Fig. 2B, one-sample Wilcoxon signed rank test vs. 33.3% chance level, p=0.002 for each nostril condition). There were no significant differences in odor identification performance between the left versus right, nor between the uni-nostril and bi-nostril conditions (two-sample Wilcoxon signed rank test, p>0.05 for all comparisons).

Finally, we asked if subjects could discern from which nostril the stimuli were delivered (Fig. 2C). Subjects could only designate bi-nostril trials above chance level (left nostril 31.9% ± 5.8%, right nostril 28.5% ± 8.5%, bi-nostril; 59.0% ± 7.2%, one-sample Wilcoxon signed rank test vs 33.3% chance level, p>0.05, p>0.05, and p=0.006, respectively). The laterality judgment was significantly better for bi-nostril trials versus uni-nostril trials but there were no significant differences between the left and right nostril trials (two-sample Wilcoxon signed rank tests, p=0.01 and p>0.05 respectively).

Overall, our behavioral results show that subjects can detect and identify odors well above chance level in all nostril configurations, with the bi-nostril condition showing a small but significant advantage in odor detection and odor laterality assessment compared to uni-nostril trials. Importantly, there were no significant differences in task performance between left and right nostrils, suggesting that neither the left nor the right nostril had a relative advantage in odor detection, odor identification, or laterality assessment.

Better disambiguation of PC odor representations correlates with successful odor identification

Prior to comparing PC responses across ipsilateral, contralateral, and bilateral odor stimuli, we first sought to confirm that odors elicit oscillations in PC and that the spectrotemporal characteristics of these responses vary across odor types, as observed in our previous studies[26,27]. Single neuron studies in rodents and neuroimaging work in humans have shown that distinct odorants induce neural activity with distinct spatiotemporal profiles in PC[28–31]. In line with these observations, recent iEEG studies by our group have shown that PC oscillatory patterns also vary across odorants, and that differences in the frequency, power, and timing of odor-induced oscillations can be used to decode odor identity[26,27].

To assess the presence of odor-induced oscillations, we aligned trials to sniff onsets and conducted time-frequency analysis for each subject, averaging across all odor types and nostril conditions. Across subjects, there were robust odor-induced responses in theta (3-8 Hz; z-scored power 2.94 ± 1.07) as well as in the beta/gamma frequency range (20-120 Hz; 1.36 ± 0.46; one-sample Wilcoxon signed rank test vs. 0, $p < 0.025$), consistent with other human PC recordings by our group[26,27] and others[32,33]. Group-level time-frequency plots averaged across all subjects are shown in Fig. 3A (see Supplementary Fig. 1 for plot linearly-scaled across frequency).

Spectrotemporal features of odor-induced oscillations varied across odor types at the level of single subjects (representative example shown in Fig. 3B). To determine if odor identity could be decoded from odor-induced oscillations at the single trial level, we implemented a three-way classifier for each PC electrode, following the methods from our previous work[26,27]. Specifically, as odor-induced responses were observed across a broad frequency range, we trained the classifier using the spectrotemporal features of oscillations between 3 and 120 Hz, and assessed model performance using a leave-one-out cross-

validation method. Statistical significance of decoding accuracy for each electrode was computed via a non-parametric, permutation-based test where the odor labels were shuffled to create a null distribution (see Methods). For the sub-set of bilateral odor trials, odor identity could successfully be decoded in at least one PC electrode in 9/10 subjects (one-tailed permutation test, $p < 0.025$). The percentage of electrodes with significant decoding was 48.2% ± 9.0% across all subjects (Fig. 3C).

As odor decoding accuracy was variable across subjects (e.g., Fig. 3C), we examined whether this variation was systematically related to odor identification performance on a subject-by-subject basis. By computing a Pearson's correlation between odor identity decoding accuracy and odor identification performance across all subjects, we found that the two variables were strongly correlated (Fig. 3D, left panel, using mean decoding accuracy across PC electrodes for each subject, Pearson's Correlation, $r=0.65$, $p=0.04$. Right panel, using the maximum decoding accuracy across PC electrodes, $r=0.68$, $p=0.03$).

In summary, consistent with our earlier work[26,27], we show that odor identity can be decoded from the spectrotemporal features of PC neural oscillations. Importantly, the data presented here expand upon our earlier findings by providing novel evidence that greater disambiguation of PC odor representations correlates with improved odor identification performance.

Speed of odor coding in PC depends on stimulus laterality

We next investigated if the speed and accuracy of odor coding in PC differs depending on whether odor information arises from the ipsilateral or the contralateral nostril, and if bi-nostril sampling enhances the speed and accuracy of odor coding relative to uni-nostril sampling. To assess the temporal evolution of odor coding in PC, we computed odor decoding accuracy for each PC electrode in a time-resolved fashion, using 200-ms sliding windows with 50% overlap (see Methods). Trials were grouped into ipsilateral, contralateral, and bilateral conditions based on the route of odor delivery with respect to each PC electrode. For example, for electrodes in the left hemisphere, left nostril odor trials were categorized as ipsilateral and right nostril odor trials were categorized as contralateral conditions and vice versa for the electrodes in the right hemisphere. Importantly, to control for inter-subject variability in inhalation length, we normalized the time axis with respect to each subject's inhalation duration such that 0% and 100% correspond to the onset and offset of inhalation, respectively. Limiting the analysis window to the inspiratory phase for each subject also ensured that our analysis was not confounded by potential re-entry of odorants into the nose upon exhalation, through the retronasal pathway[34]. We then averaged the time-resolved decoding accuracy values across subjects using percentage of inhalation duration as the time axis.

Average decoding accuracy across subjects revealed striking differences in the relative time course of odor coding across the bilateral, ipsilateral, and contralateral conditions within the time span of a single sniff (Fig. 4). Bilateral odors were encoded earliest, followed by ipsilateral, and lastly by contralateral odors. In the bi-nostril condition, odor identity was encoded in two distinct, temporally-segregated epochs (i.e., dual coding), with the first epoch peaking at 13% (range of significant decoding: 8-18%) and the second epoch peaking at 43% of inhalation (range: 37-57%). In contrast to the bi-nostril condition, odors in either uni-nostril condition were encoded within a single epoch, albeit with distinct latencies: coding of ipsilateral odors peaked at 40% (range: 32-47%), whereas coding of contralateral odors peaked later at 66% of inhalation (range: 58-73%). The temporal epochs of statistically significant decoding were determined via a permutation-based method where a null distribution was created for each laterality condition by circular shifting of decoding accuracy values across time, followed by cluster-level correction for multiple comparisons (one-tailed permutation test, $p<0.025$; see Methods).

To confirm that conversion of the time axis from seconds to percentage of inhalation did not confound our results, we repeated the same analysis without normalizing the post-stimulus interval with

respect to each subject's inhalation duration. We found that the relative order of odor coding was preserved in this control analysis (Supplementary Fig. 2A). Furthermore, to ensure that these group-level results were not driven by outlier subjects, we computed the percentage of subjects showing significant odor identity decoding at each 200-ms time bin (Supplementary Fig. 2B). This analysis confirmed that the majority of subjects displayed the same relative temporal order of odor coding across conditions. Finally, we asked if odor decoding accuracy was significantly different across odors arising from ipsilateral, contralateral, or bilateral nostrils. We found no difference in either the mean or peak odor decoding accuracy across time at the group level (Kruskal-Wallis test, $p > 0.05$ for both tests). Overall, these findings show that stimulus laterality dictates the speed, but not the accuracy of odor coding in PC.

Ipsilateral and contralateral odors elicit similar yet distinguishable responses in PC

Our results show that ipsilateral odor representations emerge earlier than their contralateral counterparts in PC (Fig. 4). These findings raise the intriguing possibility that the same odor delivered to the ipsilateral versus contralateral nostril may ultimately elicit similar representations that are merely shifted in time. Indeed, work in rodents has shown that PC responses to ipsilateral versus contralateral odors are correlated at the neural population level[22].

To test this hypothesis, we conducted time-frequency similarity analysis (see Methods) on ipsilateral and contralateral odor responses, enabling us to assess the overall similarity between odor representations across the two conditions. By training a classifier with trials from one condition (e.g., ipsilateral) and testing the accuracy of the model using trials from the other condition (e.g., contralateral), we were able to quantify the similarity between the two conditions for each PC electrode in a time-resolved fashion. This analysis was conducted independently for all possible pairs of training and testing time bins tiling the inhalation period. The prediction here is that if the responses are similar to one another at a given training/testing time point, then the classifier trained on one condition (e.g., ipsilateral) should successfully decode odor identity when tested with odor responses from the other condition (e.g., contralateral).

The resulting group-averaged time-frequency similarity matrices (TFSM) are shown in Fig. 5. Values along the diagonal correspond to decoding accuracy from training and testing at the same time points (e.g., train and test at 40% of inhalation), whereas the off-diagonal values show decoding accuracy from training and testing at different time points (e.g., train at 40%, and test at 80%). We also computed the TFSM by reversing the training and testing conditions (i.e., train on contralateral and test on ipsilateral) to identify robust, bidirectional representational similarity (Fig. 5B). Because we were interested in the representational similarity between two epochs that were temporally staggered (i.e., off-diagonal values in the TFSM), we computed the contrast between the two TFSMs in Fig 5A and 5B to eliminate the on-diagonal values. The statistical significance of the resulting matrix was assessed via a permutation test, where decoding accuracy values were circularly shifted across either training or testing time (Fig. 5C). We found that ipsilateral responses occurring at 41-59% of inhalation could decode contralateral responses occurring later at 67-94% of inhalation, as shown by the positive cluster above the diagonal (two-tailed permutation test, cluster-level $p < 0.05$). Likewise, we observed congruent findings for the reverse direction: contralateral responses occurring at 67-88% of inhalation could decode ipsilateral representations at 41-61% of inhalation (negative cluster below the diagonal). These findings support our hypothesis that the same odor arising from the contralateral nostril generate similar but delayed representations in PC compared to its counterpart arising from the ipsilateral nostril.

Finally, we considered that the strong similarity between the ipsilateral and contralateral odor coding epochs (Fig. 5) does not preclude the possibility that these odor representations could nonetheless be differentiable on a fine-grained level. We extracted spectrotemporal features from the intervals with significant odor decoding. We limited the analysis window to epochs of significant odor coding to ensure that the differences in the latency of odor coding did not influence the comparison between the ipsilateral

and contralateral odor representations (see Methods). A two-way classifier was then trained to decode stimulus laterality (ipsilateral versus contralateral) based on these spectrotemporal features. We assessed model accuracy using a leave-one-out cross validation technique, and found that oscillatory responses to ipsilateral versus contralateral odors could be classified in at least one electrode in 7/10 patients (one-tailed permutation test, $p < 0.025$; Fig. 5D). Across subjects, decoding was significant in 28.97% ± 7.44% of electrodes. Taken together, these results demonstrate that the same odor arising from the ipsilateral versus the contralateral nostril induces similar yet distinguishable representations that emerge at different epochs within the inhalation.

Dual coding of bi-nostril odors arises from temporal segregation of ipsilateral and contralateral odor inputs

In contrast to uni-nostril odors, bi-nostril odors were encoded in two temporally-segregated epochs within a single sniff (i.e., dual coding; Fig. 4). Interestingly, the temporal distance between these two epochs closely matched the time lag between the ipsilateral and contralateral coding epochs in the uni-nostril conditions (29% versus 26% of the inhalation duration, respectively). Based on these observations, we asked if the two non-overlapping epochs observed in the bi-nostril condition emerge from the temporal segregation of ipsilateral and contralateral inputs. We reasoned that if our hypothesis is true, then responses within the first coding epoch in the bi-nostril condition should resemble the responses within the ipsilateral coding epoch, whereas responses occurring in the second coding epoch should instead resemble the contralateral coding epoch. To assess the similarity of coding epochs across conditions we applied the time-frequency similarity analysis described above and compared odor coding in the bi-nostril condition with odor coding in the ipsilateral or contralateral conditions. Specifically, the classifier was trained on bilateral odor responses and tested independently on ipsilateral or contralateral odor responses across all possible training and testing time points throughout inhalation. Similar to our approach in Fig. 5, the training and testing sets were reversed for each comparison (Supplementary Fig. 3), and statistical significance was assessed on the resulting contrast matrices (two-tailed permutation test, cluster-level $p<0.05$). We found that bi-nostril responses at 12-34% of inhalation could decode ipsilateral responses at 43-65% of inhalation (Fig. 6A). Moreover, bi-nostril responses occurring later at 39-69% of inhalation could decode contralateral responses at 57-93% of inhalation (Fig. 6B). Importantly, the mirror-symmetric clusters above and below the diagonal lines indicate that reversing the training and testing conditions replicated the same results for both analyses; ipsilateral responses at 41-65% could decode bilateral representations at 9- 41%, and contralateral responses at 57-92% could decode bilateral representations at 21-65%.

Stimulus laterality dictates the timing of behaviorally-relevant odor coding

We next asked if the order of odor coding (i.e., bilateral, ipsilateral, and contralateral) affected when PC odor representations became relevant for odor identification. To address this question, we computed Pearson's correlations between decoding accuracy and task performance across subjects in a time-resolved manner. This analysis is similar to the correlation shown in Fig. 3D, except the correlations are computed independently at each time bin within each laterality condition (Supplementary Fig. 4).

We found that decoding accuracy significantly correlated with odor identification performance for all three nostril conditions, but at distinct time points (Fig. 7). Significant correlations were observed at 33-47%, 49-66%, and 65-75% of the inhalation period for bilateral, ipsilateral, and contralateral conditions, respectively, with peak correlations occurring at 40%, 54%, and 70% of inhalation (one-tailed permutation test, cluster-level $p<0.025$). These results establish that the order of correlations recapitulated the order of odor coding across conditions. Notably, in all three conditions, correlations with behavior arose later during the inhalation period compared to the onset of the corresponding odor coding epochs. For instance, bi-nostril odor coding emerged as early as 8% of inhalation but significant correlations between bi-nostril odor coding and odor identification arose at 33% of inhalation. Similarly, the onset of significant correlations were delayed by 17% and 7% of the inhalation for ipsilateral and contralateral

conditions, respectively. Lastly, while bilateral odors were encoded in two non-overlapping epochs (occurring at 8-18% and 37-57% of inhalation, as shown in Fig. 4), correlations with behavior occurred within a single epoch at 33-47% of inhalation. Together these data underscore the idea that just as stimulus laterality dictates the speed of odor coding in PC, stimulus laterality also affects how rapidly PC odor representations are able to inform subsequent odor identification.

DISCUSSION

One key feature that binds the olfactory systems of all mammals, including humans, is the presence of two nostrils, each conveying a potentially unique snapshot of the external olfactory world. Here, using iEEG recordings and machine learning methods, we show that odor information from each nostril is encoded independently in primary olfactory cortex of humans, through temporal segregation of odor inputs across nostrils, all within a single sniff. Furthermore, we demonstrate that across subjects, greater differentiation among PC odor representations scales with improved odor identification. Lastly, we show that the nostril-dependent order of odor coding also influences when PC odor coding informs odor identification.

Temporal segregation of ipsilateral and contralateral odor inputs within a single sniff

In the uni-nostril condition, we found that ipsilateral odors are encoded earlier than contralateral odors by 26% of the inhalation duration, which corresponds to 478 ms on average. Although ipsilateral and contralateral odors were encoded at different phases of inhalation, we found that stimulating either nostril with the same odor elicited similar yet distinguishable representations during their respective coding epochs. Early work in anesthetized rats has shown that odor responses in PC can be nostril-specific[21], suggesting that a given odorant may activate different neurons across PC depending on stimulus laterality. Recent work in awake mice has found that neural population responses to ipsilateral versus contralateral odorants were indeed distinguishable but remained highly correlated[22]. Our results are consistent with these rodent studies, and together suggest that ipsilateral and contralateral odors activate partially overlapping but distinct ensembles of neurons that ultimately give rise to similar yet distinguishable response dynamics at the population level.

Interestingly, the temporal distance between ipsilateral and contralateral coding epochs in the uni-nostril condition was preserved when the same odorant was delivered to both nostrils simultaneously (29% of the inhalation duration, and 498 ms on average), providing PC with temporally individuated snapshots of odor information from each nostril within one sniff. While the encoding of bi-nostril odors recapitulated the temporal pattern expected from combining the ipsilateral and contralateral coding epochs, there was one important difference: in the bi-nostril condition, epochs corresponding to ipsilateral and contralateral nostrils emerged earlier than their uni-nostril counterparts by 24% and 21% of the inhalation duration, respectively. Why simultaneous stimulation of bilateral epithelia gives rise to faster odor coding than stimulation of just one epithelium remains unclear. One marked difference of course is that each nostril received the same amount of odor in the bi-nostril trials, effectively resulting in subjects receiving twice the amount of odorant overall. It is possible that this increase in the total amount of odorant may result in faster odor coding. However, if the observed effect resulted from the olfactory system merely summating information across the two nostrils, then we would also expect this summation to result in a singular temporal epoch of odor coding, representing unified information across the two nostrils in PC. Instead, our results show that information from each nostril is encoded separately at non-overlapping time intervals within inhalation, suggesting that the olfactory system is not merely summating odor information across nostrils. Hence, the faster onset of odor coding observed in the bi-nostril condition is unlikely to be driven by the mere increase in the total amount of odorant.

It is important to note that the temporal difference in encoding of ipsilateral versus contralateral odors is not driven by differences in odor input across the two nostrils. For each odor type and experimental session, stimuli delivered to the left and right nostrils were calibrated using a photo-

ionization detector to ensure that stimuli were matched in concentration, speed of delivery, and flow rate. Furthermore, since there were no external cues indicating the site of odor delivery in a given trial, and the subjects received constant and identical air flow in both nostrils throughout all trials, the observed results cannot be explained by potential sensory or anticipatory cues biasing attention to either nostril and altering odor coding in a nostril-specific fashion. Additionally, each nostril condition (ipsilateral, contralateral, and bilateral) contains the same number of trials from electrodes in the left and right hemispheres and hence any differences that may exist across the left and right PCs are unlikely to account for differences in odor coding latencies. Finally, a potential factor that may contribute to the observed temporal differences between ipsilateral and contralateral odor coding is nasal cycling. It has been shown that one nostril typically has greater airflow and the nostril with increased airflow alternates every few hours in humans[35,36]. While we did not measure nasal cycling, it is possible that differences in nasal air flow may also influence the speed of odor coding in PC. However, since our results are pooled across subjects and includes data from both left and right hemispheres, it is unlikely that any potential nasal cycling effects, which should be randomly distributed across subjects and nostrils, would yield a consistent bias for faster coding of ipsilateral odors.

While our experiment cannot speak directly to the mechanisms underlying the temporal difference between ipsilateral and contralateral odor coding, recent studies in rodents suggest that information from ipsilateral versus contralateral nostrils may reach PC through distinct pathways (as summarized in Dalal et. al.[16]). Ipsilateral inputs are just two synapses removed from PC, as olfactory sensory neurons project to the ipsilateral olfactory bulb, which then project directly to the ipsilateral PC. Contralateral inputs, on the other hand, can follow one of two pathways to reach PC, via the so-called direct and indirect pathways, each requiring three or more synapses between the contralateral nostril and PC[16,19,20]. These differences potentially explain why ipsilateral and contralateral inputs may not reach PC simultaneously. In fact, early work using non-invasive approaches in humans have shown that responses to ipsilateral odors arise faster in the ipsilateral hemisphere compared to contralateral odors[37–39]. Notably however, these studies focused on the onset of odor-evoked activity, as opposed to onset of odor coding, and furthermore did not investigate how these temporal differences influenced sensory convergence in the bi-nostril condition.

Odor coding latency dictates time-course of behavioral correlations

PC is thought to be a critical region in encoding odor identity information and informing odor object perception[10]. Perhaps not surprisingly then, we observed that better disambiguation among odor-induced activity patterns in PC correlated with improved odor identification performance across subjects. Furthermore, the temporal order of time-resolved correlations between odor coding and behavioral performance mimicked the order of odor coding across nostril conditions: bi-nostril odor coding informed odor identification first, followed by ipsilateral, and lastly by contralateral odors. However, the time course of correlations between odor coding and odor identification was different than the time course of odor coding *per se*, in two important ways. First, for all three conditions, the behavioral correlations emerged later than the corresponding encoding epoch and second, in the bi-nostril condition, there was only a single epoch in which odor coding correlated with behavior. These observations suggest that PC odor representations influence downstream computations and odor identification with a time lag of 16% of the inhalation duration (corresponding on average to 275 ms) and furthermore imply that even though bi-nostril odors are encoded in two distinct epochs, these odor codes may nonetheless inform behavior within a singular epoch.

Altogether, our findings have important implications for odor coding in the olfactory system and provide evidence that human PC maintains distinct representations of odor information arising from each nostril through temporal segregation within a single sniff. If PC can temporally segregate identical odor inputs that arrive simultaneously to both nostrils, how then do naturally occurring differences in the timing, concentration or identity of odor inputs across the two nostrils affect odor coding in PC? Finally,

these results raise the question of whether the human olfactory system, akin to the auditory system using interaural time differences to localize sounds[40], can engage such a coding scheme to compare odor inputs across nostrils and aid in rapid odor localization within a single sniff.

ACKNOWLEDGMENTS
The authors thank the patients who participated in this experiment and the staff at the Hospital of University of Pennsylvania Epilepsy Monitoring Unit for their assistance. This work was supported by NIDCD grant R01DC018075 (J.A.G) and NINDS Kirschtein NRSA T32 postdoctoral grant (A.I.Y).

AUTHOR CONTRIBUTIONS
Conceptualization, G.N.D, K.A.D, J.A.G; methodology, G.N.D, A.I.Y, N.S; data analysis, A.I.Y and G.N.D; resources, T.L, H.I.C, K.A.D, J.A.G; writing, G.N.D, A.I.Y, J.A.G; visualization, G.N.D, A.I.Y; supervision, J.A.G.

DECLARATION OF INTERESTS
The authors declare no competing interests.

FIGURE LEGENDS
Figure 1. Experimental paradigm.
(A) Experimental setup. Two small tubes were positioned ~1 mm inside the nose to provide independent stimulation to each nostril. Airflow to each nostril was kept constant at 2L/min throughout the entire experiment across all trials and conditions. A computer controlled olfactometer delivered odorants to one or both of the nostrils by opening the appropriate valve(s) for the trial condition.

(B) Task structure. Top panel; Trials began with a fixation cross, followed by a countdown and cue to sniff. Subjects received one of three distinct odors or odorless air for 1.5 seconds. After each stimulus, subjects were asked to identify the odorant. In a subset of trials, subjects were also asked to identify which side the stimuli were delivered from. Middle panel; example uni-nostril odor delivery to the left nostril. Valve switches from odorless air to odorant for the left nostril and from odorless air to a second channel of odorless air for the right nostril. Note that both left and right nostril valves switch simultaneously and maintain the same airflow within each nostril. Bottom panel; example bi-nostril odor delivery.

(C) PC electrode locations shown on MRI images overlaid with electrode contact points. Left, position of PC electrodes shown on coronal sections in two representative subjects with unilateral and bilateral PC electrodes, respectively. Each colored dot represents one contact point on a depth electrode and the contacts positioned in PC are circled in white. Right, all PC electrode contacts across subjects depicted on an average MNI-152 brain. Colors represent PC contacts from individual subjects.

Figure 2. Behavioral performance.
Task performance on odor detection **(A)**, odor identification **(B)**, and laterality judgment **(C)** for each condition. Left and right nostril trials were averaged to illustrate behavioral performance across both uni-nostril conditions. In **(A-C)**, horizontal dashed lines indicate chance level accuracy of 50%, 33%, and 33%, respectively. Colored circles indicate data from individual subjects. Statistical significance of behavioral performance across nostril conditions was tested with Wilcoxon signed rank test. Asterisk indicates $p<0.05$ and n.s. indicates $p>0.05$.

Figure 3. Behaviorally-relevant odor-induced oscillatory responses.
(A) Odor-induced oscillations in PC. Group-level spectrogram depicting the grand-average odor response across all odor types and nostril conditions. Plot is aligned to onset of inhalation during odor delivery. See also Fig. S1.

(B) Odor identity-specific oscillations. Example spectrograms from a single subject illustrating distinct patterns of oscillatory responses to each of the three odor types delivered in the experimental session (citral, coffee, eucalyptus).

(C) Odor identity decoding accuracy across all subjects and PC electrodes. Dashed line indicates theoretical chance level of 33%. Larger circles indicate electrodes with statistically significant decoding (one-tailed permutation test, $p < 0.025$; see Methods).

(D) Accuracy of odor coding in PC correlates with successful odor identification. For each subject, the mean (left panel) or maximum decoding accuracy (right) was computed across all PC electrodes. Both decoding and behavioral accuracy were computed on the subset of bi-nostril trials, and a Pearson's correlation was computed across subjects. Colors indicate data from individual subjects. Line shows linear fit.

Figure 4. Time-course of odor-identity coding in PC depends on stimulus laterality.
Time course of decoding accuracy for each laterality condition. Electrode-level raw decoding accuracy values were z-score normalized prior to computing the group-average where the values were further normalized with respect to null distributions constructed with random shifts across time. Temporal clusters of statistically significant decoding accuracies are indicated with solid dots (one-tailed permutation test, cluster-level $p<0.025$; see Methods). Shaded area represents s.e.m.. Time axis is shown as percentage of inhalation duration. See also Fig. S2.

Figure 5. Similarity and distinguishability of ipsilateral vs contralateral odor responses.
(A-C) Time-frequency similarity matrices (TFSM) constructed by training on ipsilateral and testing on contralateral odor trials **(A)**, or training on contralateral and testing on ipsilateral odor trials **(B)**. Classifiers were trained and tested independently across all pairs of time bins tiling the inhalation duration. Values along the diagonal lines correspond to time bins where the classifier was trained and tested at the same time points. The contrast between the TFSMs in **(A, B)** is shown in **(C)**, where decoding accuracies were further normalized with respect to null distributions constructed by randomly shifting across training and testing times. Significant clusters are outlined (two-tailed permutation test, cluster-level $p<0.05$). Time represented as percentage of inhalation durations (as in Fig. 4). See Results, Methods and Fig. S3 for additional details.

(D) Representations of ipsilateral and contralateral odors during the temporal clusters shown in **(C)** were similar, yet distinguishable. Time-frequency patterns of ipsilateral and contralateral odors from their respective time intervals of odor-identity coding were submitted to a two-way classifier. Statistically significant decoding (one-tailed permutation test, $p<0.025$) of stimulus laterality was observed in at least one PC electrode in 7/10 subjects. Circles represent decoding accuracy from individual PC electrodes (color coded for individual subjects), and larger circles indicate statistical significance. Horizontal dashed line indicates chance-level accuracy of 50%.

Figure 6. Dual coding of bi-nostril odors emerges from temporal segregation of ipsilateral and contralateral odor inputs.
Contrast of time-frequency similarity matrices (TFSM) computed for bilateral vs. ipsilateral odor responses **(A)**, and for bilateral vs. contralateral odor responses **(B)**. Significant clusters are outlined (two-tailed permutation test, cluster-level $p <0.05$. See Fig. S3 for details.

Figure 7. Speed of behaviorally-relevant odor coding depends on stimulus laterality.
Group-level time course of correlations between odor decoding accuracy and odor identification performance. At each time point, a Pearson's correlation was computed between odor decoding accuracy

and behavioral accuracy across all subjects. Correlation coefficients were normalized with respect to null distributions constructed by shuffling behavioral accuracy values across subjects, and then further normalized with respect to null distributions constructed by shifting correlation values across time (see Methods). Temporal clusters of statistically significant correlations indicated with solid dots (one-tailed permutation test, cluster-level $p<0.025$). Shaded area represents s.e.m.

METHODS

Experimental Model and Subject Details

Intracranial EEG recordings from human PC were obtained from ten subjects (S1-10, 2 male, mean age 30.9 years, range 23-47 years) with drug-resistant epilepsy who were implanted with depth electrodes for pre-surgical localization of seizure foci. Data were recorded from the Hospital of the University of Pennsylvania. Informed consent was obtained from all subjects in accordance with the local Institutional Review Boards.

Data acquisition

Electrode placement decisions were made exclusively on clinical grounds, and typically focused on areas in the medial temporal lobe. Overall, five subjects had bilateral piriform cortex (PC) electrodes, one subject had right-sided electrodes only, and four subjects had left-sided electrodes only. Implanted depth macro-electrodes (Adtech AG, Frankfurt, Germany; Model SD10R-SP05X-000) were of the following specifications: each lead had 8 or 12 cylindrical platinum electrode contacts, with 2.4 mm of exposed surface, and a 2.6 mm gap between contacts. Data were acquired using a 256-channel Natus recording system (Natus Medical Incorporated, Pleasanton, CA). For each subject, signals were sampled between 500 and 2000 Hz at the physician's discretion. Respiratory airflow data were simultaneously collected using a piezoelectric pressure sensor attached to a nasal cannula (Salter Labs, Vista, CA).

Electrode selection

After co-registering the pre-operative high-resolution MRI with the post-operative CT using a linear affine registration[41], electrodes were localized in native space, and then transformed to Montreal Neurological Institute (MNI) space for visualization across all subjects on an average MNI-152 brain. Electrodes in PC were then determined based on visual comparison with manually-drawn regions of interest in MNI space. The number of PC electrodes across subjects were 7.40 ± 0.50 [5, 9] (mean ± s.e.m. [min, max]).

Behavioral paradigm

We devised an olfactory task in which individual odor stimuli was presented through one of three stimulus routes (laterality): left nostril, right nostril, or both nostrils (bi-nostril). Odor trials were interspersed with trials in which odorless air was delivered to both nostrils. For uni-nostril odor trials, odorless air was delivered to the contralateral nostril to ensure both nostrils received the same air flow. In each odor trial, the delivered odor was selected pseudo-randomly from a set of three unique and discriminable odor types, which was delivered via a stimulus route that was also pseudo-randomly selected. Hence, this paradigm ensured that subjects did not have any sensory or cognitive cues about the identity or laterality of the upcoming odor stimuli prior to its delivery. For each subject, the three odor types utilized for the entire experiment were selected from the following set: banana, citrus, orange, peanut butter, coffee, pine, and eucalyptus. Odor sets were different across subjects to ensure the results were generalizable to many odorants and were not driven by odorant-specific effects. Stimuli were administered via a custom-built, twelve-channel olfactometer, with two additional channels delivering clean air. The olfactometer was controlled using a computer equipped with MATLAB (MathWorks, Natick, MA), and the experiment was designed and administered using the PsychToolbox package[42]. For each odor type, the concentration of the odorant for the left and right nostril delivery was identical and delivered at the same air dilution rate. Furthermore, prior to each experiment, odors were tested and calibrated with a photo-ionization detector (miniPID, Aurora Scientific) to ensure that the onset latency

and peak intensity of odorants were the same for each odor type across the left and right nostril delivery setup.

Each trial began with a fixation cross, after which subjects were cued to sniff. This baseline period lasted five seconds overall, after which subjects sampled the stimulus for 1.5 seconds. During the experiment, each subject underwent a total of approximately 170 trials, of which 15-25% were odorless air trials. Of the remaining trials, each unique odor type and stimulus route occurred in equal proportions.

After stimulus delivery, subjects performed up to two judgments, the first of which was presented 3.25-4 seconds after odor onset. First, subjects were provided with the labels of all three odor types as well as the option of "no odor," and asked to identify the stimulus (across subjects, response time [RT] 3.92 ± 0.72 s). Second, for a pseudo-randomly selected subset of trials (approximately 30 trials across both odor and odorless air trials), subjects then reported whether the stimulus was delivered to the left, right, or both nostrils (RT 7.91 ± 2.54 s).

Behavioral performance was assessed for odor detection, odor identification, and stimulus laterality. Detection accuracy was calculated for the sub-set of trials in which subjects received an odor (chance-level accuracy 50%). Identification accuracy was computed for the sub-set of odor trials in which the presence of an odor was not missed (e.g., did not answer "no odor" when orange was presented). Hence, incorrect answers were those in which the delivered odor was detected, but misclassified (e.g., answer "coffee" when pine was presented), resulting in a chance-level accuracy of 33.3%. Finally, to determine laterality accuracy, we calculated the percentage of correct responses in trials where the subject correctly detected the presence of an odor (chance-level accuracy 33%).

Data pre-processing

All data were analyzed offline in MATLAB using custom scripts in conjunction with functions from the EEGLAB toolbox[43]. Data were down-sampled to 500 Hz (after an anti-alias filter), and then high-pass filtered at 0.1 Hz using a two-way least-squares zero phase-lag finite impulse response (FIR) filter (eegfilt.m). Data were then notch-filtered at 60 Hz and its harmonics to remove line noise using a second-order infinite-impulse response (IIR) filter. We visually inspected all channels to eliminate channels with significant interictal epileptiform discharges. All extra-parenchymal electrodes were also eliminated based on visual inspection of electrodes in each subject's native MRI space. Finally, we rejected noisy and flat channels in which the mean magnitude of the signal (mean of the absolute value of raw amplitudes) was 3 s.d. above or below the mean (across all included intracranial electrodes), respectively. Following our previous studies[26,27], each remaining electrode's LFP signal was then referenced to the common average (i.e., average signal across all included intracranial electrodes) to reduce common noise from, e.g., volume conduction and remote field effects[44].

Further artifact rejection was conducted at the single trial level using a previously-reported event-level algorithm[45], which was designed to automatically identify artifacts such as eye-blink artifacts, sharp transients, and interictal epileptiform discharges. Specifically, for each time point, we calculated the following metrics: 1) absolute amplitude; 2) gradient (first derivative); and 3) amplitude of the data following a 150 Hz high-pass filter. Each of these metrics were then independently *z*-score normalized with respect to the electrode-specific mean and s.d. Time points in which any of these measures exceeded 5 s.d., or all three measures simultaneously exceeded 3 s.d. were marked as artifacts. Data from 100 ms before and after each of these time points were then classified as artifacts and eliminated from all analyses.

Data were aligned to the onset of sniff in the presence of odor stimuli. As the identification question was presented as early as 3.25 seconds following stimulus onset across subjects, data analysis was limited to 3

seconds following stimulus presentation. An equivalent-length baseline period was extracted from each trial ([-3, 0] s).

Respiratory data were low-pass filtered at 10 Hz and manually inspected. Odor stimulus trials in which inspiration was sub-optimal were rejected if any of the following conditions were met: 1) overlap between odor and inhalation <100 ms; 2) peak velocity of inspiration <5th percentile of the distribution of peak velocities across all odor trials (within each subject); 3) two successive rapid sniffs taken during the odor delivery period.

QUANTIFICATION AND STATISTICAL ANALYSIS

All analyses were limited to odor trials, excluding odorless air trials. All group-level results were based on one data point from each subject, taking the mean across PC electrodes within subjects, unless otherwise noted. Finally, all statistical tests were two-tailed with α = 0.05 or one-tailed with a corrected α.

Oscillatory power

For spectral analysis across time and frequency, raw traces were filtered between 1 and 200 Hz in 60 steps with center frequencies increasing logarithmically using a zero phase-lag FIR filter with 50% overlapping bandwidths. Subsequently, the Hilbert transform was applied to extract instantaneous amplitude/power at each time point and frequency bin. To investigate odor-related changes in power, we computed a two-sample *t*-statistic of the difference in power with respect to the pre-encoding baseline at each time-frequency (TF) pixel. For within-subject analyses, we resampled the minimum number of trials across electrodes 200 times (to control for variable trial numbers after artifact rejection), and then calculated the mean power difference across electrodes between the post-stimulus ([0, 3] s) and baseline periods ([-3, 0] s). Subject-level data were then *z*-score normalized with respect to a null distribution of power differences. Null distributions were constructed independently for each TF pixel, whereby the post-stimulus and baseline period labels were randomly shuffled 500 times. Subject-level power in each frequency range of interest (theta 3-8 Hz, beta/gamma 13-30-120 Hz) was quantified by selecting the frequency sub-band with the most robust odor-induced activity within each range of interest, and then taking the mean across time during the post-stimulus epoch. For depiction of group-level data, subject-level data were further normalized by dividing by the maximum power across time and frequency prior to taking the average across subjects. For single-channel, single-condition TF examples, oscillatory power was *z*-score normalized with respect to the baseline period within each frequency sub-band.

Decoding odor identity from odor-induced patterns of oscillatory activity

We performed classification of odor identity from single-trial TF patterns of odor-induced oscillatory activity using a multi-class (three-way) non-linear support vector machine (SVM) with a radial basis function kernel[46]. As odors were randomly selected from a set of three unique odor types, chance-level accuracy is 33.3%. Following our previous studies[26,27], we developed classifier models independently for each electrode.

To extract TF features, we used the same parameters as in the TF plots: mean power in each frequency sub-band spanning the frequency range of interest (40 sub-bands spanning 3-120 Hz) was calculated across non-overlapping 10 ms windows tiling the post-stimulus epoch ([0, 3] s). To reduce computational cost, we averaged over contiguous frequency sub-bands (resulting in 20 sub-bands).

Model performance for each electrode was quantified using a leave-one-out cross-validation technique to train on all but one random set of trials from each of the three odor type classes, and tested on the left-out set of trials. We repeated this procedure 200 times and reported the mean of the resulting distribution of decoding accuracies. At each iteration, the minimum number of trials across odor types was sampled for the training set to ensure that the classifier would not be biased by differences in sample size. Statistical

significance was determined with respect to a null distribution, whereby at each iteration (N = 500), the classifier was built with permuted labels, and then used to decode for the permuted labels in the left-out set of trials. Importantly, in generating surrogate data, the feature space for each trial was not altered. Electrode-level significance was observed if the true decoding accuracy was in the top 2.5th percentile of the null distribution.

We used the subset of bi-nostril odor trials to show model performance for each PC electrode across all subjects. We also used data from the sub-set of bi-nostril odor trials for analysis of the correlation between odor identity decoding accuracy and behavioral performance on the odor identity judgment. Specifically, a Pearson's correlation was performed using the raw decoding accuracy and the raw behavioral accuracy. We note that the results were qualitatively similar when the Pearson's correlation was computed after *z*-score normalizing decoding accuracies with respect to null distributions constructed by label shuffling (as described above), and after independently *z*-score normalizing both decoding and behavioral accuracies across subjects to achieve a normal distribution. For both of these decoding analyses, data from the entire post-stimulus epoch was used to develop classifiers.

Time course of odor coding across stimulus laterality conditions

To investigate the time course of odor coding, we performed the same odor identity decoding analysis as outlined above, but in a time-resolved fashion. Features were extracted separately from 200 ms sliding windows (400 features: 20 time bins × 20 frequency bins) spanning -0.5 to 3 seconds (with respect to sniff onset) with 50% overlap, resulting in 36 decoding time bins. The time course of odor coding was compared across the following stimulus laterality conditions: 1) ipsilateral (odor delivered from ipsilateral nostril), 2) contralateral, and 3) bi-nostril. Note that in subjects with bilateral PC coverage, model performance was averaged across both left PC electrodes during left nostril stimulation and right PC electrodes during right nostril stimulation for the ipsilateral condition. Similarly, for the contralateral condition, model performance was averaged across left PC electrodes during right nostril stimulation and right PC electrodes during left nostril stimulation. Statistical testing was conducted as described above, with respect to surrogate data generated for each electrode × decoding time bin by shuffling odor identity labels across trials (N = 500). The observed electrode-level decoding accuracy values were then *z*-score normalized with respect to the corresponding surrogate distributions. To identity statistically significant temporal clusters of odor representations at the group level, we implemented a cluster-level approach[47]. For each decoding time bin, we resampled the minimum number of PC electrodes across subjects 200 times to control for variable electrode numbers across subjects, which were then averaged to generate group-level results. We then applied a one-tailed threshold of 1 s.d. within each decoding time bin, and positive cluster-level *z*-statistics were compared to a surrogate distribution (N = 500) of maximum cluster-level *z*-statistics (one-tailed, $p < 0.025$) generated by circular shifts of the observed accuracy values across time. This procedure was performed independently for each of the three stimulus laterality conditions (ipsilateral, contralateral, bi-nostril). For depiction of the number of subjects with statistically significant decoding across time, subject-level significance was observed during a time window if the average normalized decoding accuracy across electrodes was >1.96 (corresponding to a one-tailed threshold of $p < 0.025$, uncorrected across time windows).

To control for inter-subject variability in the temporal dynamics of sniff behavior, temporal clusters of significant odor decoding were also identified after normalizing time with respect to subject-specific inhalation durations, i.e., the duration from sniff onset until the end of the inhalation period (1816 ± 136 ms [1170, 2662] ms). To do this, subject-level time courses of decoding were interpolated across 100 time points that spanned each subject's mean inhalation duration (across trials) from 0 to 100%. We note that, at the group level, there was no difference between left and right nostril conditions in inhalation duration (1864 ± 138 ms vs. 1817 ± 145 ms; Wilcoxon signed rank, Z = 19, $p = 0.4$). In contrast, consistent with the literature[48], inhalation duration was longer during uni-nostril (combining trials across left and right) compared to bi-nostril odor delivery (1840 ± 140 ms vs. 1718 ± 127 ms; Z = 5, $p = 0.02$).

We therefore normalized time with respect to the mean inhalation duration (across trials) separately for the bi-nostril condition and for the two uni-nostril conditions.

Similarity of odor representations across stimulus laterality conditions

Classifier models trained with odor trials in which odors were delivered through the ipsilateral, contralateral, or bi-nostril routes were then tested on odor trials from an alternate stimulus route. Specifically, the classifier was trained with data from odor trials in which the stimulus was delivered from the ipsilateral or contralateral nostril, and then tested on patterns obtained from odors delivered from the contralateral or ipsilateral nostril, respectively (Il→Cl, Cl→Il). In addition, we trained with data from bilateral odor stimulation, and tested on patterns obtained from ipsilateral or contralateral stimulation (Bl→Il, Bl→Cl). Finally, we trained on ipsilateral or contralateral stimulation, and tested on bilateral stimulation (Il→Bl, Cl→Bl). As the time-resolved decoding analyses described above (**Time course of odor coding across stimulus laterality conditions**) suggested differential time courses of odor coding dependent on stimulus laterality, for the current set of analyses we trained and tested on data from all pairs of decoding time bins tiling the inhalation duration, resulting in a two-dimensional matrix of decoding results across training time (columns) and testing time (rows), which we refer to as the time-frequency similarity matrix (TFSM). Decoding accuracies along the diagonal of the matrix represent model performance when the model was trained and tested with data from the same decoding time bin. In contrast, values above the diagonal show the results when models trained on a prior time window were tested on future time windows, whereas values below the diagonal show results when models trained on a future time window were tested on past time windows.

To investigate the similarity of odor representations across stimulus laterality conditions, we took the difference of each pair of corresponding TFSMs, resulting in the following three TFSM contrasts: 1) Il→Cl − Cl→Il, 2) Bl→Il − Il→Bl, 3) Bl→Cl − Cl→Bl. Statistical analysis of electrode-level TFSMs were conducted mirroring the procedure described above (**Time course of odor coding across stimulus laterality conditions**). Briefly, we generated surrogate data for each electrode × training time bin × testing time bin by shuffling odor identity labels across trials (N = 500). The observed raw decoding accuracy values were then *z*-score normalized with respect to the corresponding surrogate distributions. For group-level results, we resampled the minimum number of PC electrodes across subjects for each training time bin training × testing time bin (N = 200), which were then averaged. Statistically significant temporal clusters were identified using a permutation method, in which surrogate distributions were constructed by shuffling data across either the training or testing time axes, one of which was selected randomly at each of the 500 iterations. Significance was assessed using a two-tailed threshold of greater than 0.5 s.d. or lesser than -0.5 s.d. at each training and testing time pair, and a two-tailed cluster-level threshold of $p < 0.05$.

Distinguishability of odor representations between ipsilateral versus contralateral conditions

Representations of ipsilateral and contralateral odors were used to train and test a model to distinguish between the two stimulus laterality conditions. To do this, we extracted time-frequency features from statistically significant coding epochs identified in the Il→Cl − Cl→Il contrast TFSM, during which a model trained on ipsilateral odors could classify contralateral odors, and vice versa. These temporal clusters spanned 18-27% of inhalation. To account for inter-subject variability in inhalation duration (note that the maximum inhalation duration across subjects was 2,662 ms), we chose to extract time-frequency features from a 600 ms window centered on the geometric centers of the two temporal clusters (50.5% for ipsilateral and 79% for contralateral). Classifier development and statistical analysis was performed as described above (**Decoding odor identity from odor-induced patterns of oscillatory activity**), with two important differences. The null distribution was constructed by shuffling laterality labels, not odor type labels. Laterality was classified between ipsilateral and contralateral odor trials matching trials of the same odor types.

Time-resolved behavioral correlations of PC odor representations
We performed the behavioral correlations outlined above (**Decoding odor identity from odor-induced patterns of oscillatory activity)**, but in a time-resolved manner. This analysis was performed independently for each stimulus laterality condition, so as to determine whether the accuracy of PC odor representations would be correlated with subsequent behavioral performance on the odor identification task at different time points depending on stimulus laterality. Electrode-level decoding accuracies were again normalized with respect to null distributions constructed by shuffling labels, and the mean across electrodes was computed for each subject. Then, both decoding and behavioral accuracies were independently *z*-score normalized across subjects to achieve a normal distribution, after which a Pearson's correlation was computed across all subjects. To identify statistically significant temporal clusters of correlations, the raw Pearson's correlation values at each time point were first *z*-score normalized with respect to null distributions constructed by shuffling the relative order of behavioral accuracies across subjects, while maintaining the decoding accuracies (N = 500). We then generated surrogate distributions by circular shifts of the correlation values across time (N = 500), where significance was assessed using a one-tailed 1 s.d. pixel-level threshold and a one-tailed cluster-level threshold of $p < 0.025$.

SUPPLEMENTARY FIGURE LEGENDS
Supplementary Figure 1. Group-level spectogram.
Depicted using a linear frequency scale (as opposed to the logarithmic scale shown in Fig. 3A) to emphasize oscillatory responses at higher frequencies.

Supplementary Figure 2. Speed of odor coding in PC depends on stimulus laterality.
(A) Group-level time course of odor coding for odors delivered via ipsilateral, contralateral, or bi-nostril routes depicted across raw time axis ([-0.5, 2] s with respect to sniff onset), as opposed to time normalized with respect to inhalation duration (as in Fig 4). Temporal clusters of statistically significant odor coding are shown in solid dots (one-tailed permutation test, p<0.025). Shaded area represents s.e.m.

(B) Percentage of subjects demonstrating statistically significant decoding within [-0.5, 2] s with respect to sniff onset. Subject-level statistical significance was determined by comparing the mean decoding accuracy across all electrodes with respect to a null distribution constructed by shuffling odor labels (uncorrected across time, p<0.025; see Methods).

Supplementary Figure 3. Illustration of time-frequency similarity analysis for bi-nostril odor representations.
Time-frequency similarity matrices (TFSM) were computed by training the classifier on bilateral odor responses and testing on ipsilateral (top left) or contralateral (bottom left) odor responses, across all possible training and testing time bins tiling the inhalation duration. We also performed the same computation after reversing the training and testing sets (middle column). We then took the contrast of corresponding pairs of TFSMs (right column, also shown in Fig. 6). Significant clusters are outlined (two-tailed permutation test, p<0.05).

Supplementary Figure 4. Illustration of time-resolved correlation analysis of decoding accuracy and behavioral performance.
Pearson's correlations were computed between odor decoding accuracy and behavioral accuracy in the odor identification judgment across all subjects. The time course of these correlations is shown for each laterality condition in Fig. 7. Here, we show the correlations at two representative time points for the bilateral condition (left column). Pearson's correlation was 0.0 at 19% of inhalation, and increased to 0.88 at 36%. The observed Pearson's correlations at these two time points are shown with the corresponding null distributions (right column), which were constructed by shuffling behavioral accuracies across subjects (see Methods).

REFERENCES

1. Rigolli, N., Magnoli, N., Rosasco, L. & Seminara, A. Learning to predict target location with turbulent odor plumes. *eLife* **11**, e72196 (2022).
2. Connor, E. G., McHugh, M. K. & Crimaldi, J. P. Quantification of airborne odor plumes using planar laser-induced fluorescence. *Exp. Fluids* **59**, 137 (2018).
3. Celani, A., Villermaux, E. & Vergassola, M. Odor Landscapes in Turbulent Environments. *Phys. Rev. X* **4**, 041015 (2014).
4. Crimaldi, J. P. & Koseff, J. R. High-resolution measurements of the spatial and temporal scalar structure of a turbulent plume. *Exp. Fluids* **31**, 90–102 (2001).
5. Porter, J. *et al.* Mechanisms of scent-tracking in humans. *Nat Neurosci* **10**, 27–9 (2007).
6. Rats Smell in Stereo. https://www.science.org/doi/10.1126/science.1122096 doi:10.1126/science.1122096.
7. Gardiner, J. M. & Atema, J. The function of bilateral odor arrival time differences in olfactory orientation of sharks. *Curr Biol* **20**, 1187–91 (2010).
8. Catania, K. C. Stereo and serial sniffing guide navigation to an odour source in a mammal. *Nat. Commun.* **4**, 1441 (2013).
9. Wu, Y., Chen, K., Ye, Y., Zhang, T. & Zhou, W. Humans navigate with stereo olfaction. *Proc. Natl. Acad. Sci.* **117**, 16065–16071 (2020).
10. Gottfried, J. A. Central mechanisms of odour object perception. *Nat. Rev. Neurosci.* **11**, 628–641 (2010).
11. Uchida, N., Poo, C. & Haddad, R. Coding and Transformations in the Olfactory System. *Annu. Rev. Neurosci.* **37**, (2013).
12. Brann, D. H. & Datta, S. R. Finding the Brain in the Nose. *Annu. Rev. Neurosci.* **43**, 277–295 (2020).
13. Blazing, R. M. & Franks, K. M. Odor coding in piriform cortex: mechanistic insights into distributed coding. *Curr. Opin. Neurobiol.* **64**, 96–102 (2020).

14. Isaacson, J. S. Odor representations in mammalian cortical circuits. *Curr. Opin. Neurobiol.* **20**, 328–331 (2010).

15. Kay, L. M. *et al.* Olfactory oscillations: the what, how and what for. *Trends Neurosci.* **32**, 207–214 (2009).

16. Dalal, T., Gupta, N. & Haddad, R. Bilateral and unilateral odor processing and odor perception. *Commun Biol* **3**, 150 (2020).

17. *The synaptic organization of the brain, 5th ed*. xiv, 719 (Oxford University Press, 2004). doi:10.1093/acprof:oso/9780195159561.001.1.

18. Kucharski, D., Burka, N. & Hall, W. G. The anterior limb of the anterior commissure is an access route to contralateral stored olfactory preference memories. *Psychobiology* **18**, 195–204 (1990).

19. Russo, M. J., Franks, K. M., Oghaz, R., Axel, R. & Siegelbaum, S. A. Synaptic Organization of Anterior Olfactory Nucleus Inputs to Piriform Cortex. *J Neurosci* **40**, 9414–9425 (2020).

20. Grobman, M. *et al.* A Mirror-Symmetric Excitatory Link Coordinates Odor Maps across Olfactory Bulbs and Enables Odor Perceptual Unity. *Neuron* **99**, 800-813 e6 (2018).

21. Wilson, D. A. Binaral interactions in the rat piriform cortex. *J Neurophysiol* **78**, 160–9 (1997).

22. Grimaud, J., Dorrell, W., Pehlevan, C. & Murthy, V. *Bilateral Alignment of Receptive Fields in the Olfactory Cortex*. http://biorxiv.org/lookup/doi/10.1101/2020.02.24.960922 (2020) doi:10.1101/2020.02.24.960922.

23. Kucharski, D. & Hall, W. G. New Routes to Early Memories. *Science* **238**, 786–788 (1987).

24. Savic, I. & Gulyas, B. PET shows that odors are processed both ipsilaterally and contralaterally to the stimulated nostril. *NeuroReport* **11**, 2861–2866 (2000).

25. Porter, J., Anand, T., Johnson, B., Khan, R. M. & Sobel, N. Brain mechanisms for extracting spatial information from smell. *Neuron* **47**, 581–92 (2005).

26. Jiang, H. *et al.* Theta Oscillations Rapidly Convey Odor-Specific Content in Human Piriform Cortex. *Neuron* **94**, 207-219.e4 (2017).

27. Yang, A. I. *et al.* The what and when of olfactory working memory in humans. *Curr. Biol.* **31**, 4499-4511.e8 (2021).

28. Stettler, D. D. & Axel, R. Representations of Odor in the Piriform Cortex. *Neuron* **63**, 854–864 (2009).

29. Roland, B., Deneux, T., Franks, K. M., Bathellier, B. & Fleischmann, A. Odor identity coding by distributed ensembles of neurons in the mouse olfactory cortex. *eLife* **6**, e26337 (2017).

30. Pashkovski, S. L. *et al.* Structure and flexibility in cortical representations of odour space. *Nature* **583**, 253–258 (2020).

31. Schoonover, C. E., Ohashi, S. N., Axel, R. & Fink, A. J. P. Representational drift in primary olfactory cortex. *Nature* **594**, 541–546 (2021).

32. Yang, Q. *et al.* Smell-induced gamma oscillations in human olfactory cortex are required for accurate perception of odor identity. *PLOS Biol.* **20**, e3001509 (2022).

33. Zhou, G. *et al.* Human olfactory-auditory integration requires phase synchrony between sensory cortices. *Nat. Commun.* **10**, 1168 (2019).

34. Small, D. M., Gerber, J. C., Mak, Y. E. & Hummel, T. Differential Neural Responses Evoked by Orthonasal versus Retronasal Odorant Perception in Humans. *Neuron* **47**, 593–605 (2005).

35. Kahana-Zweig, R. *et al.* Measuring and Characterizing the Human Nasal Cycle. *PLoS One* **11**, e0162918 (2016).

36. Hasegawa, M. & Kern, E. B. The human nasal cycle. *Mayo Clin. Proc.* **52**, 28–34 (1977).

37. Tonoike, M. *et al.* Ipsilateral dominance of human olfactory activated centers estimated from event-related magnetic fields measured by 122-channel whole-head neuromagnetometer using odorant stimuli synchronized with respirations. *Ann N Acad Sci* **855**, 579–90 (1998).

38. Lascano, A. M., Hummel, T., Lacroix, J. S., Landis, B. N. & Michel, C. M. Spatio-temporal dynamics of olfactory processing in the human brain: an event-related source imaging study. *Neuroscience* **167**, 700–8 (2010).

39. Stadlbauer, A. *et al.* Spatiotemporal Pattern of Human Cortical and Subcortical Activity during Early-Stage Odor Processing. *Chem Senses* **41**, 783–794 (2016).

40. Grothe, B., Pecka, M. & McAlpine, D. Mechanisms of Sound Localization in Mammals. *Physiol. Rev.* **90**, 983–1012 (2010).

41. Smith, S. M. *et al.* Advances in functional and structural MR image analysis and implementation as FSL. *NeuroImage* **23**, S208–S219 (2004).

42. Brainard, D. H. The Psychophysics Toolbox. *Spat. Vis.* **10**, 433–436 (1997).

43. Delorme, A. & Makeig, S. EEGLAB: an open source toolbox for analysis of single-trial EEG dynamics including independent component analysis. *J. Neurosci. Methods* **134**, 9–21 (2004).

44. Li, G. *et al.* Optimal referencing for stereo-electroencephalographic (SEEG) recordings. *NeuroImage* **183**, 327–335 (2018).

45. Staresina, B. P. *et al.* Hierarchical nesting of slow oscillations, spindles and ripples in the human hippocampus during sleep. *Nat. Neurosci.* **18**, 1679–1686 (2015).

46. LIBSVM: A library for support vector machines: ACM Transactions on Intelligent Systems and Technology: Vol 2, No 3. https://dl.acm.org/doi/abs/10.1145/1961189.1961199.

47. Maris, E. & Oostenveld, R. Nonparametric statistical testing of EEG- and MEG-data. *J. Neurosci. Methods* **164**, 177–190 (2007).

48. Sobel, N., Khan, R. M., Hartley, C. A., Sullivan, E. V. & Gabrieli, J. D. Sniffing longer rather than stronger to maintain olfactory detection threshold. *Chem Senses* **25**, 1–8 (2000).

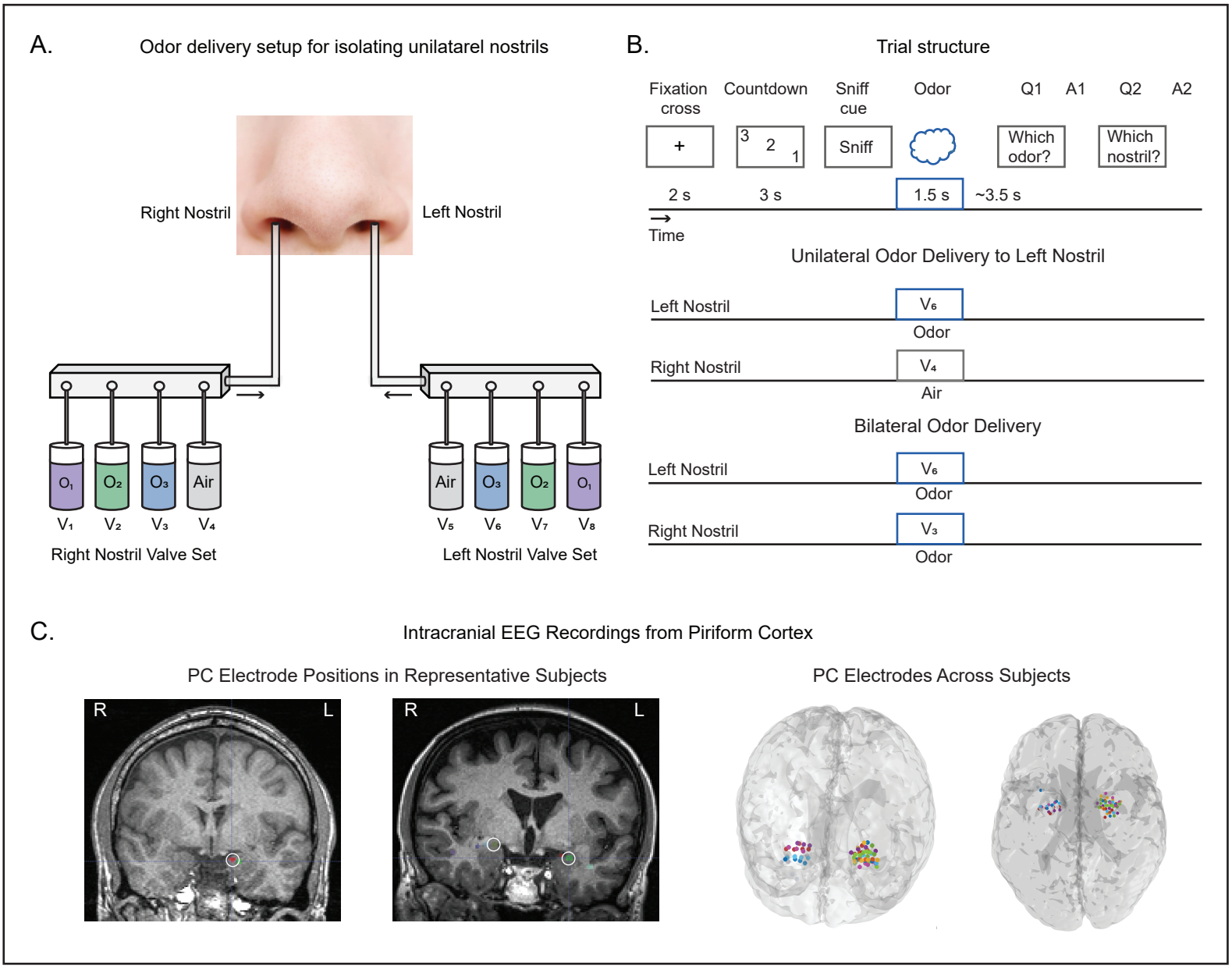

Figure 1. Experimental paradigm.
(A) Experimental setup. Two small tubes were positioned ~1 mm inside the nose to provide independent stimulation to each nostril. Airflow to each nostril was kept constant at 2L/min throughout the entire experiment across all trials and conditions. A computer controlled olfactometer delivered odorants to one or both of the nostrils by opening the appropriate valve(s) for the trial condition.

(B) Task structure. Top panel; Trials began with a fixation cross, followed by a countdown and cue to sniff. Subjects received one of three distinct odors or odorless air for 1.5 seconds. After each stimulus, subjects were asked to identify the odorant. In a subset of trials, subjects were also asked to identify which side the stimuli were delivered from. Middle panel; example uni-nostril odor delivery to the left nostril. Valve switches from odorless air to odorant for the left nostril and from odorless air to a second channel of odorless air for the right nostril. Note that both left and right nostril valves switch simultaneously and maintain the same airflow within each nostril. Bottom panel; example bi-nostril odor delivery.

(C) PC electrode locations shown on MRI images overlaid with electrode contact points. Left, position of PC electrodes shown on coronal sections in two representative subjects with unilateral and bilateral PC electrodes, respectively. Each colored dot represents one contact point on a depth electrode and the contacts positioned in PC are circled in white. Right, all PC electrode contacts across subjects depicted on an average MNI-152 brain. Colors represent PC contacts from individual subjects.

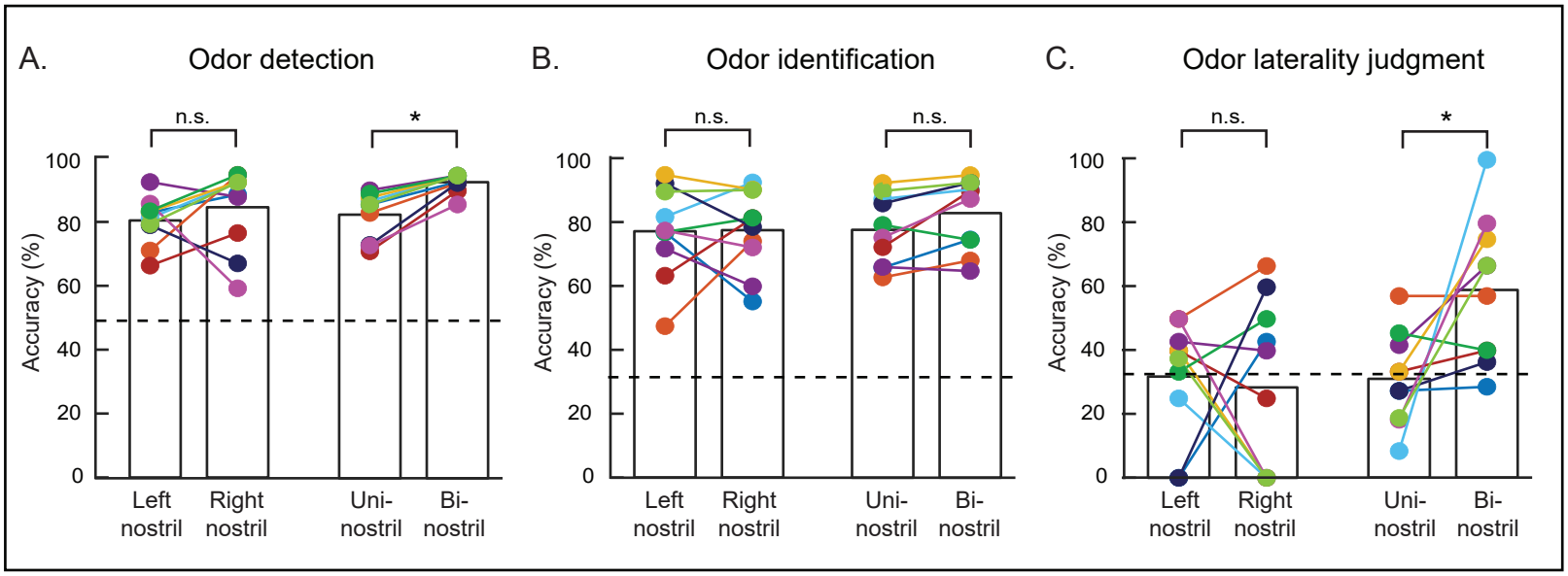

Figure 2. Behavioral performance.
Task performance on odor detection **(A)**, odor identification **(B)**, and laterality judgment **(C)** for each condition. Left and right nostril trials were averaged to illustrate behavioral performance across both uni-nostril conditions. In **(A-C)**, horizontal dashed lines indicate chance level accuracy of 50%, 33%, and 33%, respectively. Colored circles indicate data from individual subjects. Statistical significance of behavioral performance across nostril conditions was tested with Wilcoxon signed rank test. Asterisk indicates $p<0.05$ and n.s. indicates $p>0.05$.

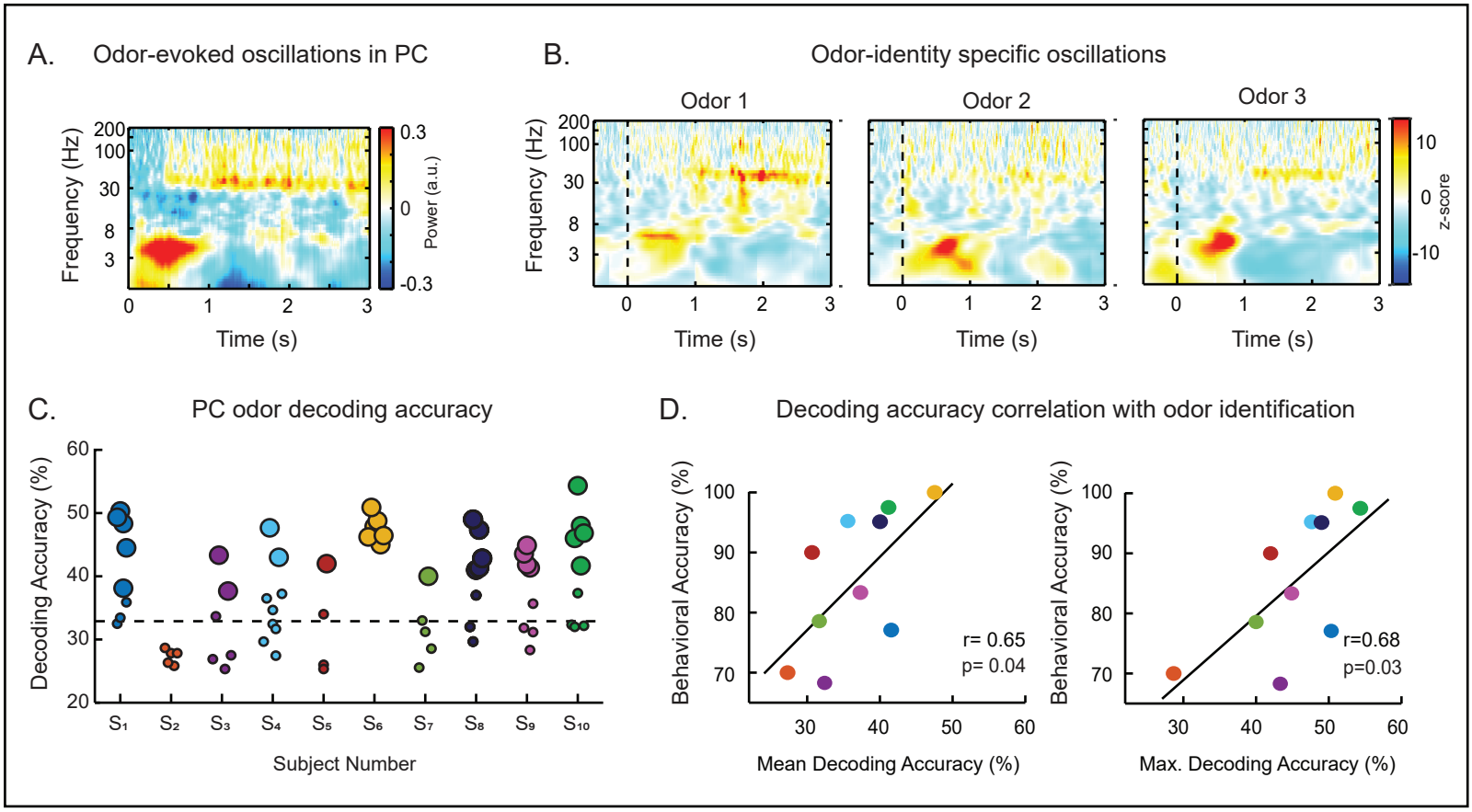

Figure 3. Behaviorally-relevant odor-induced oscillatory responses.
(A) Odor-induced oscillations in PC. Group-level spectrogram depicting the grand-average odor response across all odor types and nostril conditions. Plot is aligned to onset of inhalation during odor delivery. See also Fig. S1.

(B) Odor identity-specific oscillations. Example spectrograms from a single subject illustrating distinct patterns of oscillatory responses to each of the three odor types delivered in the experimental session (citral, coffee, eucalyptus).

(C) Odor identity decoding accuracy across all subjects and PC electrodes. Dashed line indicates theoretical chance level of 33%. Larger circles indicate electrodes with statistically significant decoding (one-tailed permutation test, $p < 0.025$; see Methods).

(D) Accuracy of odor coding in PC correlates with successful odor identification. For each subject, the mean (left panel) or maximum decoding accuracy (right) was computed across all PC electrodes. Both decoding and behavioral accuracy were computed on the subset of bi-nostril trials, and a Pearson's correlation was computed across subjects. Colors indicate data from individual subjects. Line shows linear fit.

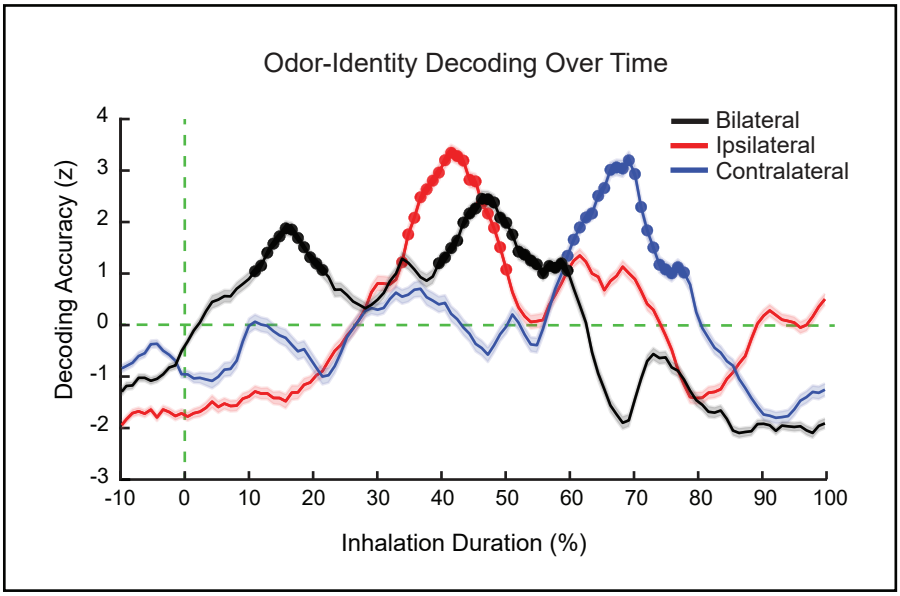

Figure 4. Time-course of odor-identity coding in PC depends on stimulus laterality.
Time course of decoding accuracy for each laterality condition. Electrode-level raw decoding accuracy values were z-score normalized prior to computing the group-average where the values were further normalized with respect to null distributions constructed with random shifts across time. Temporal clusters of statistically significant decoding accuracies are indicated with solid dots (one-tailed permutation test, cluster-level $p<0.025$; see Methods). Shaded area represents s.e.m.. Time axis is shown as percentage of inhalation duration. See also Fig. S2.

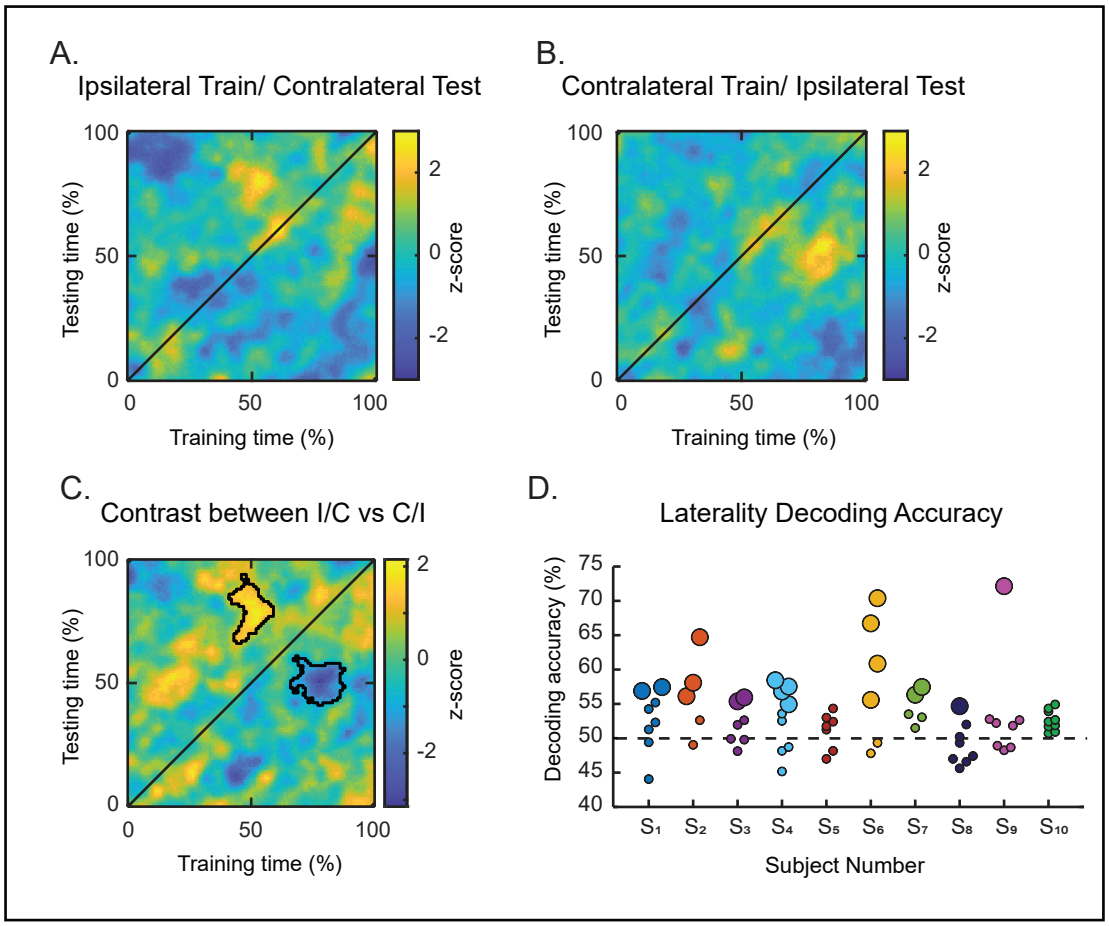

Figure 5. Similarity and distinguishability of ipsilateral vs contralateral odor responses. **(A-C)** Time-frequency similarity matrices (TFSM) constructed by training on ipsilateral and testing on contralateral odor trials **(A)**, or training on contralateral and testing on ipsilateral odor trials **(B)**. Classifiers were trained and tested independently across all pairs of time bins tiling the inhalation duration. Values along the diagonal lines correspond to time bins where the classifier was trained and tested at the same time points. The contrast between the TFSMs in **(A, B)** is shown in **(C)**, where decoding accuracies were further normalized with respect to null distributions constructed by randomly shifting across training and testing times. Significant clusters are outlined (two-tailed permutation test, cluster-level $p<0.05$). Time represented as percentage of inhalation durations (as in Fig. 4). See Results, Methods and Fig. S3 for additional details.

(D) Representations of ipsilateral and contralateral odors during the temporal clusters shown in **(C)** were similar, yet distinguishable. Time-frequency patterns of ipsilateral and contralateral odors from their respective time intervals of odor-identity coding were submitted to a two-way classifier. Statistically significant decoding (one-tailed permutation test, $p<0.025$) of stimulus laterality was observed in at least one PC electrode in 7/10 subjects. Circles represent decoding accuracy from individual PC electrodes (color coded for individual subjects), and larger circles indicate statistical significance. Horizontal dashed line indicates chance-level accuracy of 50%.

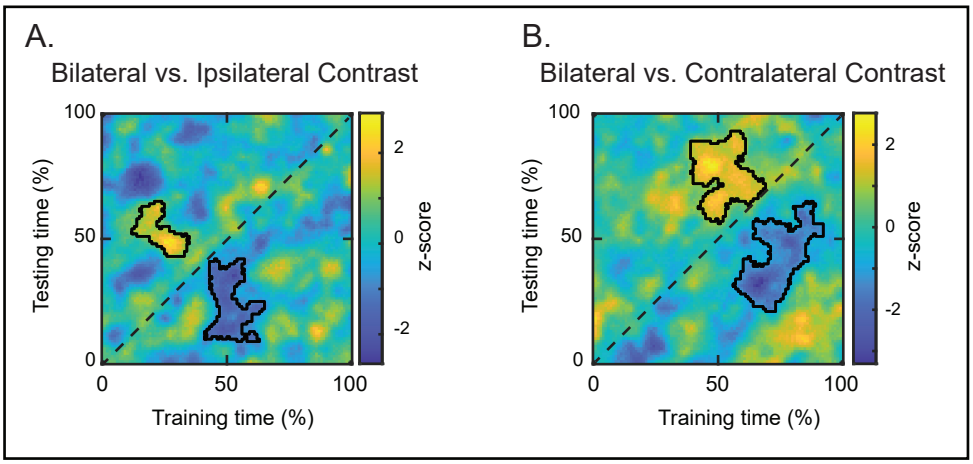

Figure 6. Dual coding of bi-nostril odors emerges from temporal segregation of ipsilateral and contralateral odor inputs.
Contrast of time-frequency similarity matrices (TFSM) computed for bilateral vs. ipsilateral odor responses **(A)**, and for bilateral vs. contralateral odor responses **(B)**. Significant clusters are outlined (two-tailed permutation test, cluster-level $p < 0.05$. See Fig. S3 for details.

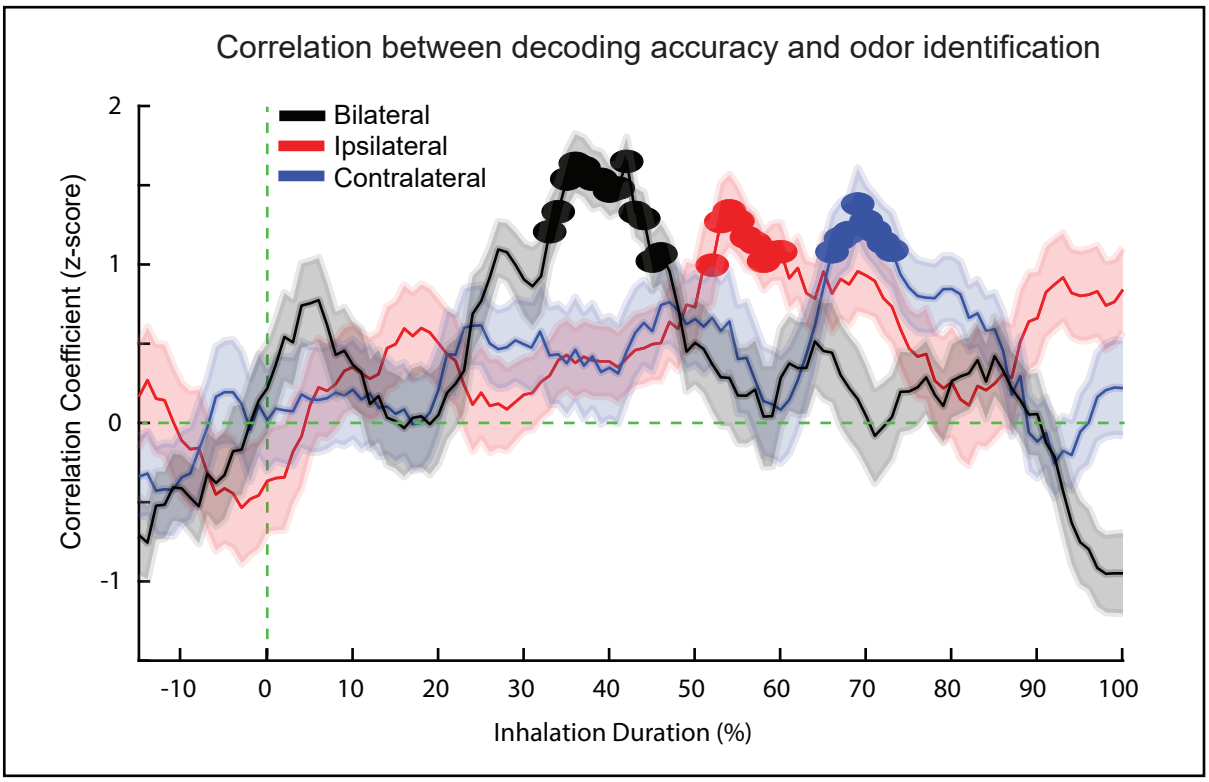

Figure 7. Speed of behaviorally-relevant odor coding depends on stimulus laterality.
Group-level time course of correlations between odor decoding accuracy and odor identification performance. At each time point, a Pearson's correlation was computed between odor decoding accuracy and behavioral accuracy across all subjects. Correlation coefficients were normalized with respect to null distributions constructed by shuffling behavioral accuracy values across subjects, and then further normalized with respect to null distributions constructed by shifting correlation values across time (see Methods). Temporal clusters of statistically significant correlations indicated with solid dots (one-tailed permutation test, cluster-level $p<0.025$). Shaded area represents s.e.m.